

# A 28–30 GHz CMOS Reflection-Type Phase Shifter With Full 360° Phase Shift Range

Ali Basaligheh<sup>ID</sup>, *Student Member, IEEE*, Parvaneh Saffari<sup>ID</sup>, *Student Member, IEEE*,  
Soroush Rasti Boroujeni<sup>ID</sup>, *Student Member, IEEE*, Igor Filanovsky<sup>ID</sup>, *Life Senior Member, IEEE*,  
and Kambiz Moez<sup>ID</sup>, *Senior Member, IEEE*

**Abstract**—This brief presents a millimeter-wave passive reflection-type phase shifter (RTPS) capable of producing a 360° phase shift range with low insertion loss (IL) in 28–30 GHz range. The circuit consists of a 90° Lange coupler and two multi-resonance loads where a switched inductor and CMOS varactors are employed. As opposed to previously reported RTPS requiring multiple control voltages, the proposed reflective load requires only one control voltage for the varactors which results in simplicity and reduced dc power consumption of the control blocks. Fabricated in 65 nm CMOS process, this RTPS achieves a measured average insertion loss of 9.5 dB at 29 GHz while consuming zero dc power. The RTPS occupies only 388 × 615 μm<sup>2</sup> of chip area.

**Index Terms**—Millimeter-wave phased-array, reflection type phase shifter, switching inductor, varactor, CMOS technology.

## I. INTRODUCTION

MILLIMETER-WAVE (mm-wave) phased array systems are widely used for fifth-generation (5G) cellular communication above 28 GHz to overcome the existing high radiation path loss and improve the signal to noise (SNR) ratio by enabling electrical beam steering [1]. Phase shifters (PSs) are the key part of a phased array system and can be categorized as active and passive types. These PSs should cover a 360° phase shift in order to be employed in phased arrays with large scan angles while exhibiting low insertion loss (IL) and low gain/loss variation. For scalability, the reduction in dc power consumption and implementation in small chip areas is necessary [2].

Vector-modulator based active PSs provide gain and high phase resolution but suffer from nonlinearity, high noise figure (NF) and consume dc power [3]–[7]. Conversely, passive PSs are very linear, and can be subdivided into three main configurations: 1) Switched type phase shifter (STPS),

2) Loaded-line phase shifter (LLPS) and 3) Reflection type phase shifter (RTPS). In the STPS, by switching between the high-pass/low-pass signal paths or switching between the transmission lines with different electrical length, discrete phase shifts with large steps (e.g., 180°, 90°, and 45°) can be achieved [8]–[10]. Using an increased number of stages with reduced size of each step (e.g., 22.5° or 11.25°) is leading to higher IL and excessive chip area due to the switching loss at mm-wave frequencies and bulky passive elements, respectively. In LLPS utilizing lumped-component based transmission line with zero dc power the achieved phase shift range is usually lower than 45° because of the limited tuning range of MOS varactors at mm-wave frequencies. Cascading multiple stages degrades the IL substantially [2], [11].

RTPS's, in addition to zero dc power consumption and superior linearity, demonstrate continuous phase shift range with moderate chip sizes [12]–[17]. Total phase shift range of an RTPS is determined by the reflective loads which are usually realized by LC components. However, a 360° phase shift range along with low IL cannot be achieved by employing conventional C-L-C  $\pi$ -loads with single control voltage [16]. Yet, several C-L-C  $\pi$ -loads proposed recently help to obtain a full 360° phase shift range. But they are utilizing two control voltages that add to the complexity and overall power consumption of the phase shifter [1] and [12].

In this brief, a new load structure is proposed to reach a 360° phase shift range along with low IL at 29 GHz and utilizing only one control voltage for tuning the loads. The proposed structure eliminates extra control circuitry, often realized with on-chip digital to analog converters (DACs), and its associated power consumption.

This brief is organized as follow: the proposed load structure and its principle of operation to achieve a 360° phase shift range are explained in Section II. Section III presents the circuit design. Section IV reports the experimental results. A conclusion is provided in Section IV.

## II. RTPS FOR MM-WAVE APPLICATIONS

### A. Principle of Operation

Fig. 1 shows the schematic diagram of a conventional RTPS [12] including an ideal 90° coupler and two tunable loads. The quadrature coupler divides the input signal into a through and coupled parts with 0° and 90° phase shifts,

Manuscript received September 26, 2019; revised October 15, 2019 and December 7, 2019; accepted January 7, 2020. Date of publication January 9, 2020; date of current version November 4, 2020. This brief was recommended by Associate Editor C. W. Sham. (Corresponding author: Ali Basaligheh.)

Ali Basaligheh, Parvaneh Saffari, Igor Filanovsky, and Kambiz Moez are with the Department of Electrical and Computer Engineering, Faculty of Engineering, Donadeo Innovation Centre for Engineering, University of Alberta, Edmonton, AB T6G1H9, Canada (e-mail: ali.basaligheh@ualberta.ca).

Soroush Rasti Boroujeni is with the Centre for Intelligent Antenna and Radio Systems, University of Waterloo, Waterloo, ON N2L 3G1, Canada.

Color versions of one or more of the figures in this article are available online at <http://ieeexplore.ieee.org>.

Digital Object Identifier 10.1109/TCSII.2020.2965395

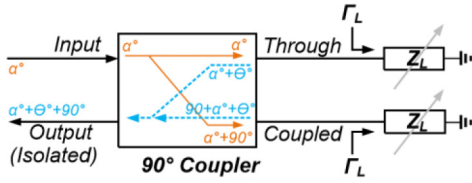


Fig. 1. Operation principle of RTPS with 3-dB coupler.

and the reflected signals from the loads will be combined in phase at the output (isolated port) resulting in the desired signal where the output phase shift  $\theta$ , total phase shift range  $\Delta\theta$ , and  $IL$  can be obtained as

$$\theta = -90 - 2\tan^{-1}\left(\frac{Z_L}{Z_0}\right) = \angle\Gamma_L, \quad (1)$$

$$\begin{aligned} \Delta\theta &= 2\left[\tan^{-1}\left(\frac{Z_{L,max}}{Z_0}\right) - \tan^{-1}\left(\frac{Z_{L,min}}{Z_0}\right)\right] \\ &= \angle\Gamma_{L,max} - \angle\Gamma_{L,min}, \end{aligned} \quad (2)$$

and

$$IL = -20\log|\Gamma_L|, \quad (3)$$

where  $Z_L$ ,  $Z_0$  and  $\Gamma_L$  are the load, characteristic impedance and reflection coefficient normalized to the  $Z_0$ , respectively. Hence, the total phase shift range of an RTPS is determined by the achievable phase range of reflection coefficient produced by tuning the load. The tunable load can be realized by a variable capacitive load (C) or series/parallel inductive-variable capacitive (L-C) tanks. They can produce a phase shift range less than 60° and 120°, respectively, assuming that the maximum to minimum capacitance ratio  $C_{max}/C_{min}$  of varactors is limited by 3 [12].

A C-L-C  $\pi$ -network shown in Fig. 2(a) where both capacitors are controlled by a single voltage can produce up to 330° phase shift with proper component sizing assuming varactors'  $\frac{C_{max}}{C_{min}}$  of 3 [1]. The RTPS proposed in [16] achieves a 360° phase shift by cascading two phase shifters each producing 180° phase shift using a symmetrical C-L-C  $\pi$ -network. To achieve a full 360° phase shift using a single RTPS, the authors in [1] and [12] proposed to use asymmetrical C-L-C  $\pi$ -networks where, in addition, each varactor is controlled independently by its own control voltage as shown in Fig. 2 (b) and (c). These load structures, however, require two separate control voltages, produced by two DACs, adding to the complexity and power consumption of the overall phase shifter. In the next section, we propose a load structure that requires a single control voltage only to achieve the full 360° phase shift range.

### B. Proposed Load for RTPS

A proposed alternative multi-resonance load structure with varactors controlled by a single voltage is shown in Fig. 2 (d). Here two inductance values are obtained by switching on/off the transformer load. This tunable inductor gives an additional degree of freedom to extend the RTPS phase shift from ~330° to 360° using a single control voltage for the varactors.

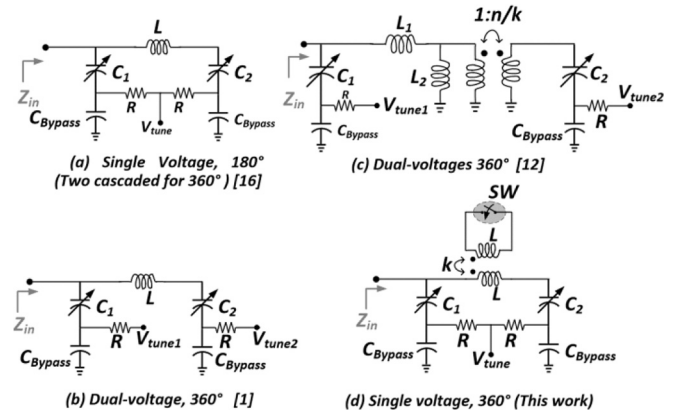


Fig. 2. Multi-resonance loads for 360° RTPS, (a) C-L-C  $\pi$ -load with asymmetric capacitors, (b) transformer-based multi-resonance load, (c) C-L-C  $\pi$ -load with 180° phase shift (2 RTPSs are cascaded to achieve 360° phase shift), (d) proposed multi-resonance load based on transformer switching.

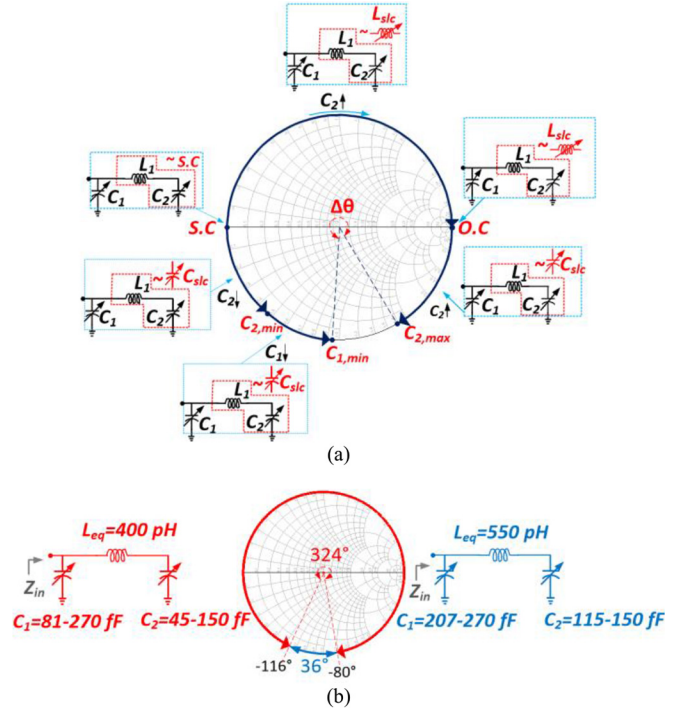


Fig. 3. Load impedance tuning range for (a) a conventional C-L-C  $\pi$ -network, (b) for the proposed load with lossless components at 28 GHz.

In the conventional C-L-C  $\pi$ -network, shown in Fig. 3(a), a series combination of  $C_2$  and  $L_1$  results in a short circuit (S.C.) at the input for the value of  $C_2$  that resonates with  $L_1$  at the frequency of operation. After this, increasing  $C_2$  produces a variable inductance ( $L_{slc}$ ) from the series combination of  $C_2$  and  $L_1$  which approaches to open circuit (O.C.) on the Smith chart when  $L_{slc}$  resonates with parallel  $C_1$ . Further increasing  $C_2$  pushes the impedance to the point which is the parallel combination of  $C_1$  and  $L_1$ , and  $C_2 = C_{2,max}$  gives a small capacitive impedance. On the other hand starting again from S.C. point, but decreasing capacitance values for  $C_2$  and  $C_1$ , moves the impedance from S.C. to  $C_{2,min}$  and  $C_{1,min}$ , respectively, resulting in a phase shift which can be around up to 330° with practical values (one can

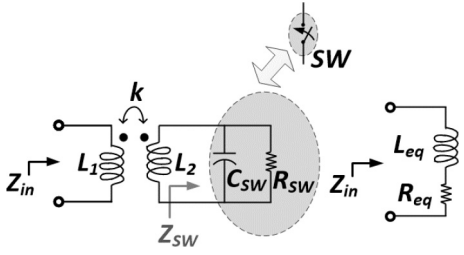


Fig. 4. Transformer loaded by a switch.

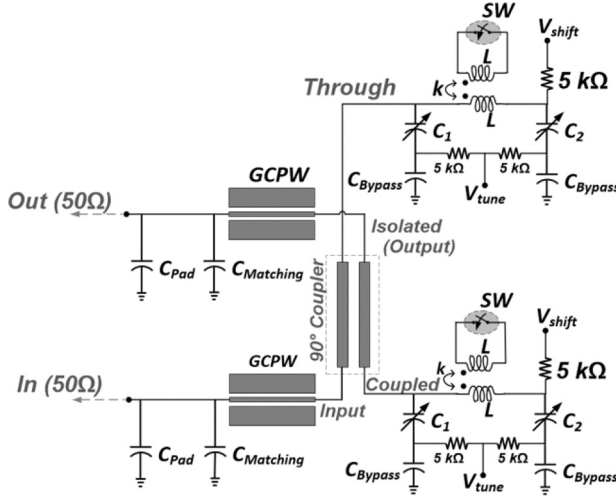


Fig. 5. Schematic of proposed RTPS.

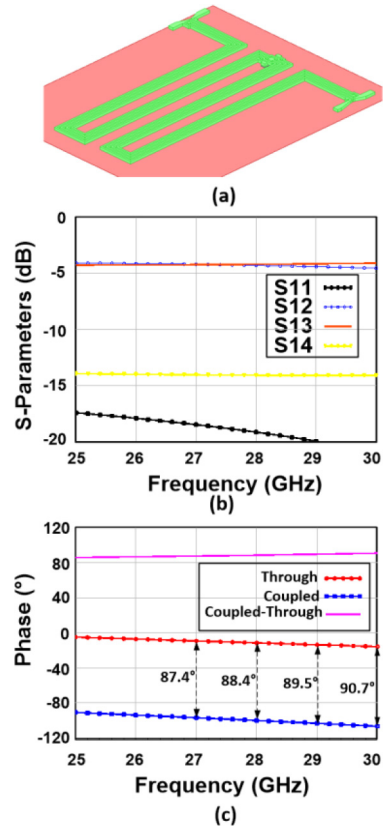
employ one control voltage for both varactors  $C_1 = kC_2$  [1]. One way to bridge the gap between the impedances at  $C_{2,\max}$  and  $C_{1,\min}$  and achieve a full  $360^\circ$  phase shift range is to control  $C_1$  and  $C_2$  independently using two control voltages as proposed in [1] and [12]. Here, we propose to change the inductance value of the symmetrical C-L-C  $\pi$ -networks such that increasing  $L_1$  pushes impedance from point  $C_{2,\max}$  to point  $C_{1,\min}$  to achieve a full  $360^\circ$  phase shift range. This method requires a single control voltage only.

To verify the effectiveness of the proposed approach, a C-L-C  $\pi$ -resonator with lossless components and a fixed inductor was designed for  $324^\circ$  phase shift range (Fig. 3 (b)). It requires  $L_{eq} = 400$  pH and  $C_1$  and  $C_2$  changing from 81-270 fF and 45-150 fF, respectively. With changing the inductor value from 400 pH to 550 pH, and keeping the same capacitors, the lower part of the Smith chart is covered for a full  $360^\circ$  phase shift range. For the mentioned inductance, only a small variation of  $C_1$  and  $C_2$  (207-270 fF and 115-150 fF) produces the required phase shift range.

To produce two inductance values, we proposed to use a transformer loaded with a switch to change its input inductance from one value to another. Using Fig. 4, one finds that the input impedance of the loaded transformer can be calculated as

$$Z_{in} = j\omega L_1 + \frac{k^2 \omega^2 L_1 L_2}{Z_{SW} + j\omega L_2}, \quad (4)$$

where the transformer is assumed to be ideal and  $L_1$ ,  $L_2$  are the primary and secondary coil inductors,  $C_{SW}$ ,  $R_{SW}$  are switch

Fig. 6. (a) 3D EM view of the  $90^\circ$  Lange coupler (b) simulated amplitude response, and (c) phase response using HFSS 3D EM simulator.

capacitor and resistor,  $k$  is the coupling factor of the coils, and  $Z_{SW}$  is given by

$$Z_{SW} = \frac{R_{SW}}{1 + j\omega C_{SW} R_{SW}}. \quad (5)$$

The equivalent inductance ( $L_{eq}$ ) and series resistance ( $R_{eq}$ ) of the loaded transformer shown in Fig. 4, can be derived as

$$L_{eq} = L_1 \frac{R_{SW}^2 (1 - \omega^2 C_{SW} L_2) [1 - \omega^2 C_{SW} L_2 (1 - k^2)] + \omega^2 L_2^2 (1 - k^2)}{R_{SW}^2 (1 - \omega^2 C_{SW} L_2)^2 + \omega^2 L_2^2}, \quad (6)$$

and

$$R_{eq} = \frac{L_1 L_2 k^2 R_{SW} \omega^2}{R_{SW}^2 (1 - \omega^2 C_{SW} L_2)^2 + \omega^2 L_2^2}. \quad (7)$$

Using (6) and (7), the quality factor ( $Q$ ) can be calculated as

$$Q = \frac{L_{eq} \omega}{R_{eq}} = \frac{R_{SW}^2 (1 - \omega^2 C_{SW} L_2) [1 - L_2 C_{SW} \omega^2 (1 - k^2)] + L_2 C_{SW} \omega^2 (1 - k^2)}{R_{SW} L_2 k^2 \omega}, \quad (8)$$

Assuming an ideal switch, when the switch is turned on ( $R_{SW} \sim 0$ ),  $L_{eq}$  becomes

$$L_{eq} = L_1 (1 - k^2), \quad (9)$$

and when the switch is turned off ( $R_{SW} \sim \infty$ ),

$$L_{eq} = L_1 \left( 1 + \frac{k^2 L_2 \omega^2 C_{SW}}{1 - L_2 \omega^2 C_{SW}} \right), \quad (10)$$



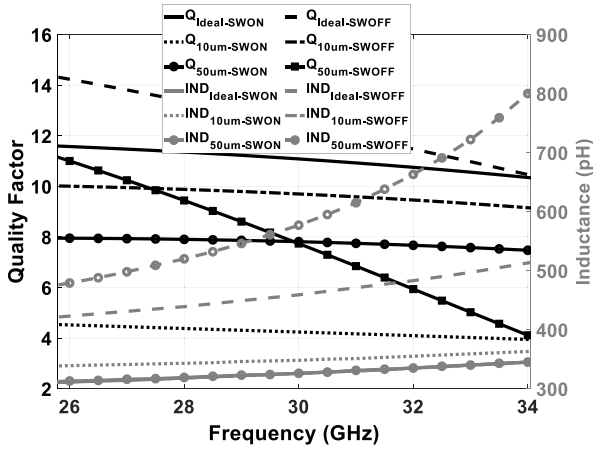


Fig. 7. Simulated Q and inductance of transformer loaded by switches with different parameters.

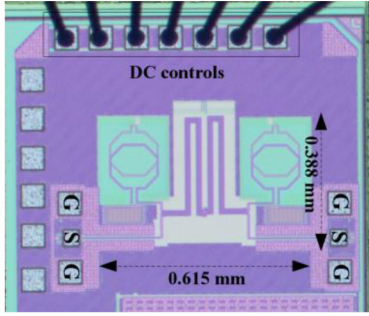


Fig. 8. Chip microphotograph of proposed RTPS.

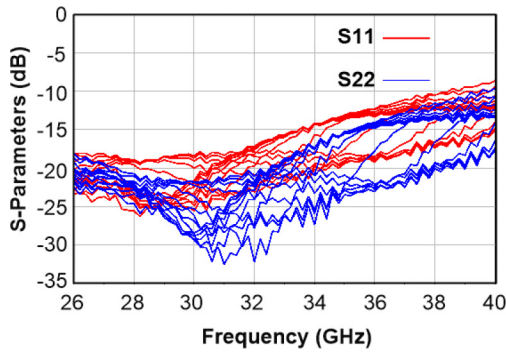


Fig. 9. Measured input and output return losses.

According to (9) and (10),  $L_{eq}$  varies by turning the load switch on and off to produce two inductor values adding an extra degree of freedom to a C-L-C  $\pi$ -resonator structure.

Hence, a C-L-C  $\pi$ -resonator with a transformer loaded by a switch may be used to provide two values of inductance required for a full 360° RTPS design.

### III. CIRCUIT DESIGN

Fig. 5 shows the schematic of the proposed mm-wave RTPS implemented in 65nm CMOS technology. The main circuit is consisting of a 90° coupler with a characteristic impedance of 35  $\Omega$  and two identical reflective loads including a transformer and two varactors ( $C_1$  and  $C_2$ ). Then the input and

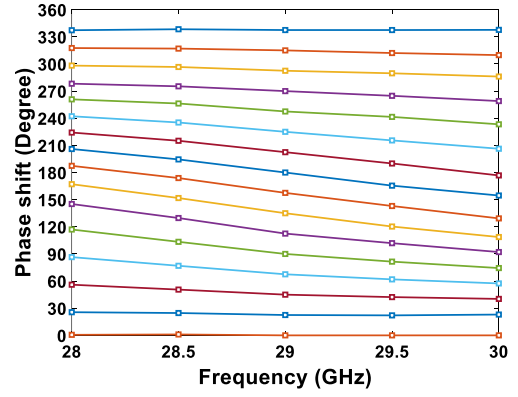


Fig. 10. Measured phase shift versus frequency.

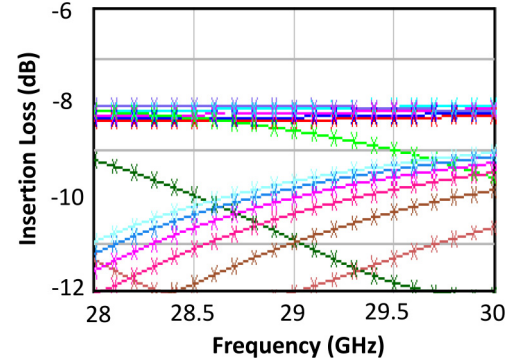


Fig. 11. Measured insertion loss versus frequency.

isolated ports of the coupler are matched to the 50  $\Omega$  by a utilizing a Grounded Coplanar Waveguide (GCPW) line and a Metal-Insulator-Metal (MIM) capacitor ( $C_{Matching}$ ) in parallel with input/output pads ( $C_{pad}$ ). Fig. 6 (a) shows the employed conventional 90° Lange coupler where the microstrip lines and ground plane are implemented by the process's top thick metal layer (3.4  $\mu\text{m}$ ) and bottom metal layer (0.18  $\mu\text{m}$ ), respectively. Fig. 6 (b) depicts the EM simulation results where the return loss and IL of better than  $-14$  dB and  $-4.2$  dB, respectively, are achieved at 28 GHz. Furthermore, the phase difference between the coupled and through ports is  $89^\circ \pm 1.7^\circ$  in 26 to 30 GHz range (Fig. 6 (c)).

The transformer was simulated in HFSS 3D EM simulator. Fig. 7 illustrates the simulations results for different switch sizes. The size of 50  $\mu\text{m}$  is corresponding to Q of 8-10 for  $L_{eq}$ . As the ON resistance of the transistor is inversely proportional to their size, the quality factor of loaded transformer with larger switches are higher. However, the increased parasitic capacitor of the larger switches will limit the resonance frequency of the inductor. Accumulation-mode CMOS varactors ( $C_1$  and  $C_2$ ) are sized for  $C_{max}/C_{min} \cong 4$  and  $Q \sim 10$  with the length and finger width of 0.35  $\mu\text{m}$  and 1.5  $\mu\text{m}$ , respectively. Size of switches were optimized to 40  $\mu\text{m}$ ,  $V_{shift}$  was fixed to 0.7 V and  $V_{tune}$  was varying from 0 to 1.2 V.

### IV. EXPERIMENTAL RESULTS

Fig. 8 shows the chip microphotograph of the implemented mm-wave RTPS in 65nm CMOS technology with an active

TABLE I  
PERFORMANCE SUMMARY AND COMPARISON AGAINST PRIOR ZERO-DC-POWER RTPS

Reference	[1] TMTT 2017	[12] TCAS-I 2018	[16] RFIC 2008	[18] IMS 2016	This work
Process	65nm CMOS	130nm BiCMOS	180nm CMOS	130nm BiCMOS	65nm CMOS
Frequency (GHz)	28	60	24	60	29
Phase shift range (°)	360°	360°	360°*	200°	360°
Control method	Dual voltages	Dual voltages	Single voltage	Single voltage	Single voltage
Input/output return loss (dB)	6.7	10.4	12	15	18
Average Insertion Loss (dB)	7.75	9.9	11.3	8.2	9.5
Chip Area (mm <sup>2</sup> )	0.16	0.16	0.33	0.28	0.23

\*Two 180° stages are cascaded.

area of  $388 \times 615 \mu\text{m}^2$ . The circuit is measured on wafer utilizing Agilent E8361C PNA and Cascade 40 GHz ground-signal-ground (GSG) Z-probes. Fig. 9 shows that the return reflection coefficients ( $S_{11}$  and  $S_{22}$ ) remain below  $-18$  dB for the entire operating frequency range. Fig. 10 demonstrates the measured phase shift range for the entire frequency band where  $V_{\text{shift}}$  is kept constant at 0.7 V and  $V_{\text{tune}}$  varies from 0 to 1.2 V.

Experimental  $IL$  versus frequency is plotted in Fig. 11 corresponding to maximum and minimum values of 7.2 dB and 11.8 dB, respectively.

The RTPS experimental results are compared with the recent state-of-art mm-wave RTPS's Table I where it shows that our proposed work is the only single-stage phase shifter that achieves a 360 phase range using a single control voltage. The other parameters of the phase shifter reported in Table I are either better than or on par with that of previously reported works.

## V. CONCLUSION

A mm-wave RTPS with full-span phase shift range of 360° is presented. The loaded-transformer is used as a switchable inductor in a C-L-C  $\pi$ -load of RTPS to extend the phase shift. Only one control voltage is used for both loads resulting in less complexity and power consumption of the control circuits. The measurement results demonstrate a 360° phase shift range with the average IL and return loss of 9.5 and  $-18$  dB over 28-30 GHz band, respectively. The chip is implemented in 65nm CMOS technology with RTPS active area of  $388 \times 615 \mu\text{m}^2$ .

## ACKNOWLEDGMENT

The authors would like to thank CMC Microsystems for chip fabrication and simulation software.

## REFERENCES

- [1] A. R. Garg and A. S. Natarajan, "A 28-GHz low-power phased-array receiver front-end with 360° RTPS phase shift range," *IEEE Trans. Microw. Theory Techn.*, vol. 65, no. 11, pp. 4703–4714, Nov. 2017.
- [2] F. Ellinger, H. Jackel, and W. Bachtold, "Varactor-loaded transmission-line phase shifter at C-band using lumped elements," *IEEE Trans. Microw. Theory Techn.*, vol. 51, no. 4, pp. 1135–1140, Apr. 2003.
- [3] Y. Yu *et al.*, "A 60-GHz 19.8-mW current-reuse active phase shifter with tunable current-splitting technique in 90-nm CMOS," *IEEE Trans. Microw. Theory Techn.*, vol. 64, no. 5, pp. 1572–1584, May 2016.
- [4] A. Asodeh and M. Atarodi, "A full 360° vector-sum phase shifter with very low RMS phase error over a wide bandwidth," *IEEE Trans. Microw. Theory Techn.*, vol. 60, no. 6, pp. 1626–1634, Jun. 2012.
- [5] S. Y. Kim, D.-W. Kang, K.-J. Koh, and G. M. Rebeiz, "An improved wideband all-pass I/Q network for millimeter-wave phase shifters," *IEEE Trans. Microw. Theory Techn.*, vol. 60, no. 11, pp. 3431–3439, Nov. 2012.
- [6] D. Pepe and D. Zito, "Two mm-wave vector modulator active phase shifters with novel IQ generator in 28 nm FDSOI CMOS," *IEEE J. Solid-State Circuits*, vol. 52, no. 2, pp. 344–356, Feb. 2017.
- [7] K.-J. Koh and G. M. Rebeiz, "0.13- $\mu\text{m}$  CMOS phase shifters for X-, Ku-, and K-band phased arrays," *IEEE J. Solid-State Circuits*, vol. 42, no. 11, pp. 2535–2546, Nov. 2007.
- [8] S. Dey and S. K. Koul, "Reliability analysis of Ku-band 5-bit phase shifters using MEMS SP4T and SPDT switches," *IEEE Trans. Microw. Theory Techn.*, vol. 63, no. 12, pp. 3997–4012, Dec. 2015.
- [9] B.-W. Min and G. M. Rebeiz, "Single-ended and differential Ka-band BiCMOS phased array front-ends," *IEEE J. Solid-State Circuits*, vol. 43, no. 10, pp. 2239–2250, Oct. 2008.
- [10] I. Kalyoncu, E. Ozeren, M. Kaynak, and Y. Gurbuz, "A 4-bit SiGe passive phase shifter for X-band phased arrays," in *Proc. IEEE Radio Wireless Symp.*, Austin, TX, USA, 2013, pp. 310–312.
- [11] S. Shamsadini, I. M. Filanovsky, P. Mousavi, and K. Moez, "A 60-GHz transmission line phase shifter using varactors and tunable inductors in 65-nm CMOS technology," *IEEE Trans. Very Large Scale Integr. (VLSI) Syst.*, vol. 26, no. 10, pp. 2073–2084, Oct. 2018.
- [12] T.-W. Li and H. Wang, "A millimeter-wave fully integrated passive reflection-type phase shifter with transformer-based multi-resonance loads for 360° phase shifting," *IEEE Trans. Circuits Syst. I, Reg. Papers*, vol. 65, no. 4, pp. 1406–1419, Apr. 2018.
- [13] C.-H. Wu, W.-T. Li, J.-H. Tsai, and T.-W. Huang, "Design of a K-band low insertion loss variation phase shifter using 0.18- $\mu\text{m}$  CMOS process," in *Proc. IEEE Asia-Pac. Microw. Conf.*, Dec. 2010, pp. 1735–1738.
- [14] B. Biglarbegan, M. R. Nezhad-Ahmadi, M. Fakhrazadeh, and S. Safavi-Naeini, "Millimeter-wave reflective-type phase shifter in CMOS technology," *IEEE Microw. Compon. Lett.*, vol. 19, no. 9, pp. 560–562, Sep. 2009.
- [15] J.-Y. Lyu, S.-C. Huang, and H.-R. Chuang, "K-band CMOS phase shifter with low insertion-loss variation," in *Proc. Asia-Pac. Microw. Conf. (APMC)*, Kaohsiung, Taiwan, 2012, pp. 88–90.
- [16] J.-C. Wu, C.-C. Chang, S.-F. Chang, and T.-Y. Chin, "A 24-GHz full-360° CMOS reflection-type phase shifter MMIC with low loss-variation," in *Proc. IEEE Radio Freq. Integr. Circuits Symp.*, Atlanta, GA, USA, 2008, pp. 365–368.
- [17] R. B. Yishay and D. Elad, "A 57–66 GHz reflection-type phase shifter with near-constant insertion loss," in *Proc. IEEE MTT-S Int. Microw. Symp. (IMS)*, San Francisco, CA, USA, 2016, pp. 1–4.